The assessment and evolution of offshore gas hydrate deposits using seafloor controlled source electromagnetic methodology

Nigel Edwards, Reza Mir, Ele Willoughby
Department of Physics, University of Toronto,
Toronto, Ontario, Canada, M5S 1A7.
Email: edwards@core.physics.utoronto.ca

Katrin Schwalenberg
BGR,
Geozentrum Hannover, Stilleweg 2,
D-30655 Hannover, Germany.

Carsten Scholl
Fugro Electro Magnetic GmbH,
Wolfener Strae 36V,
D-12681 Berlin, Germany

***Abstract*—Natural gas hydrates are ice-like solids that occur worldwide in seafloor sediments typically along active continental margins. They consist of gas molecules, mainly methane, contained in a cage-like, clathrate structure of water molecules. They form under low temperature and high pressure conditions, typically offshore in the uppermost few hundred metres of sediment in water depth exceeding about 500 m. The global abundance of methane frozen in hydrate exceeds the amount of all other known fossil hydrocarbon resources. Gas hydrates are a source of a large volume of methane gas and are recognized as an important possible future energy resource.**

Marine controlled source electromagnetic (CSEM) methods, sensitive to variations in resistivity, have become an important and valuable tool in the detection of offshore hydrate Hydrate is a resistive target. It increases the formation resistivity of a sediment layer if it forms in sufficient quantity to block previously interconnected pore spaces.

Controlled source electromagnetic (CSEM) methods depend on a simple concept of physics. If a time varying EM field is generated at or near the seafloor, then eddy currents are induced in the sea water and subjacent crust in accordance with Faraday's law. The outward progress of the currents with time depends on range and electrical conductivity of the surroundings. In particular, the apparent speed in the sea water will be slower than that in the less conductive crustal zones. Measurements at a remote location of the electric and magnetic fields associated with the eddy currents may be inverted for the crustal resistivity structure including local anomalous concentrations of hydrate.

Our CSEM system has been used successfully to map hydrate on the Cascadia Margin, to the west of Vancouver Island, British Columbia. The area, a convergent margin, is the focus of intensive studies on gas hydrates which have been identified on seismic sections, by direct sampling and from the analyses of cores and logs collected by the Ocean Drilling Programs. It has also been used in New Zealand in a similar geologic setting.

The next stage in the research is the monitoing of one of more deposits as a function of time - in this case several years. The objective is the understanding of how hydrate is formed and how it evolves. It requires the installation of equipment on the seafloor which is locally powered and which can communicate with an onshore base. Neptune Canada provides the infrastucture for the experiment. It is a Canadian subsea observatory network consisting of a cable linking several nodes to a terminal on Vancouver Island. The cable carries power and high speed ethernet interconnectivity. Instruments, including the CSEM apparatus have been connected to the nodes and data may be collected from them in real time. The CSEM array spans a known gas hydrate deposit. The engineering of both the network and the CSEM system is described together with a numerical model study.

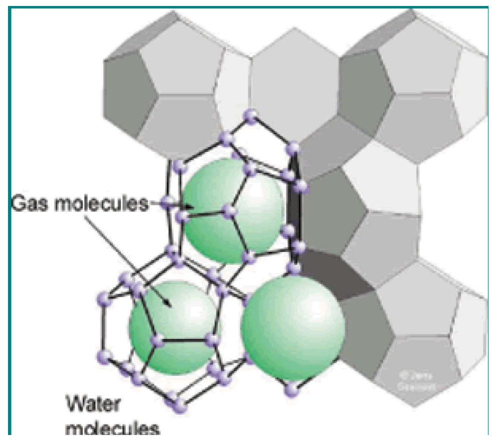

Fig. 1. A common molecular structure of gas hydrate (Structure I).

I. Methane hydrate

Methane hydrate, or clathrate, is an ice-like, white solid formed of repetitive crystalline polyhedral cages of hydrogen bonded water molecule. Most cages contain a guest methane molecule held by Van der Waals bonds, as shown in Fig. 1.

The history of the study of gas hydrates and descriptions of their physical and chemical properties are summarized in Sloan[1]. Methane hydrates occur naturally worldwide: on continental and insular slopes and rises of active and passive margins; on continental shelves of polar regions; and in deep water environments of inland lakes and seas [2]. Each volume of methane hydrate can yield up to 164 volumes of methane (STP). The amount of methane in subaquatic gas hydrates could exceed 10^{16} Kg of methane carbon [3] and consequently form an important resource. Indeed, the amount of accessible carbon in hydrate may exceed all other sources (Fig. 2). Hydrates form at appropriate temperature and pressure conditions when water is saturated with gas. They are stable within the upper several hundred meters of

978-1-4244-5222-4/10/$26.00 ©2010 IEEE

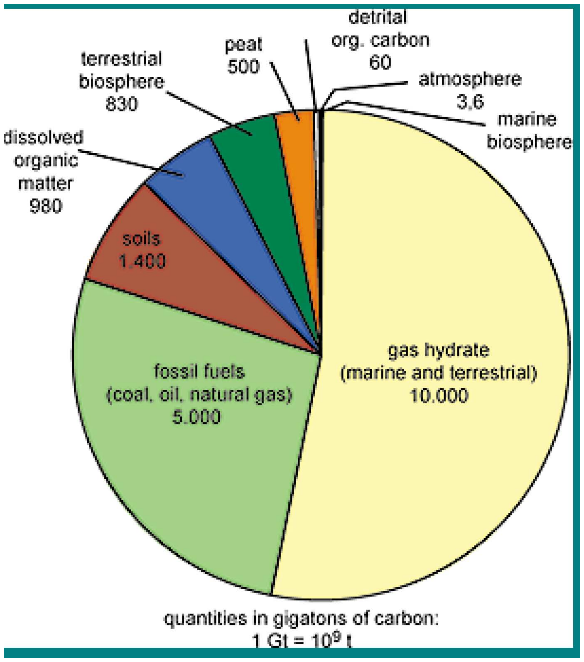

Fig. 2. Sources of accessible carbon

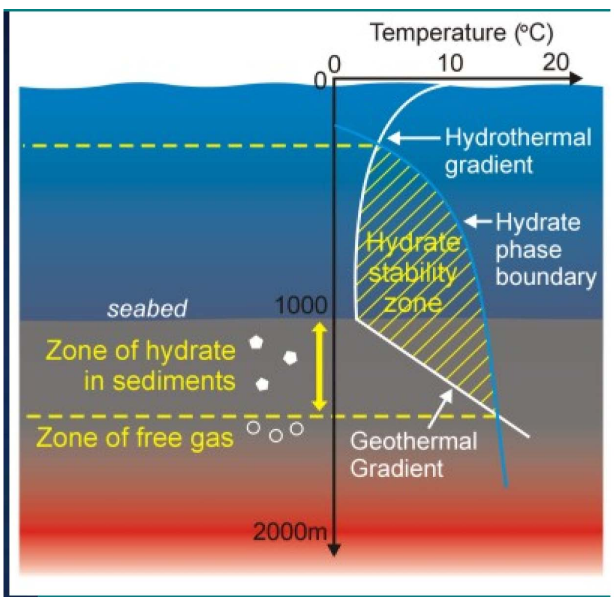

Fig. 3. The hydrate stability phase diagram

sediments below the seafloor in water depths exceeding about 500 m [4]. The phase diagram is shown in Fig. 3. The base of the stable hydrate zone is marked on seismic reflection sections by a high-amplitude, negative-polarity bright spot called the bottom simulating reflector (BSR) [5] [6] [7]. The hydrate BSR deepens with increasing water depth, varies with the geothermal gradient, and often cuts across bedding plane reflections. Methane is generated locally biogenically within the zone of hydrate stability. Methane hydrate is produced as sedimentation occurs.With ongoing sedimentation, hydrates at the base of the stability zone undergo continuous decomposition owing to changes in the isotherms. The pore water eventually becomes supersaturated and a free gas phase is produced. The gas can migrate upward back into the stable hydrate zone and reform into hydrate.

The internal structure of hydrated sediment is not clearly defined on reflection seismic sections. The total volume of hydrate and its value as a resource can therefore not be obtained directly from these data. Some sections do show a region above the BSR characterized by an abrupt drop in amplitude which may be correlated with the cementation of hydrate into the sediment according to Lee and others [8], who estimate gas hydrate content accordingly. While the effect of gas hydrate on seismic velocity is not well studied, they have suggested that hydrated sediment, 50% porosity, could show as much as a 30% increase in P-wave velocity and density compared with the hydrate free zones above it [8]. Other proposed schemes rely on the comparison of hydrated sediment physical properties measured in the laboratory with those inferred from *in situ* measurements of seismic velocity determined from wide-angle reflection surveys. Electrical logs, *in situ* measurements of electrical properties, have been used systematically to identify horizons and classify sediment types. Gas hydrate, like ice, is an insulating component. Collett [9] compiled well log responses from Prudhoe Bay and noted that an increase of 30% in acoustic velocity was associated with 30 fold increase in resistivity. The rationale for using electrical methods is therefore clear. The variability of resistivity measurement can be related to the amount of hydrate present through various empirical rules like Archie's law.

II. Resistivity and Archie's Law

Gas hydrate evaluation is based on the concept of an increased resistivity in gas hydrate-rich zones. Archie's law [10] can be used as a first order proxy to relate measured bulk resistivities to porosity estimates for a simple two-phase system that consists of the resistive grain matrix and the conductive pore fluid. Archie's law is an empirical relation which works well for heterogeneous materials, where the scale of gas hydrate inclusions is small compared with the Tx-Rx separation. In a general form, it is

$$\rho_f = a\rho_w\phi^{-m}, \tag{1}$$

where ρ_f is the measured formation resistivity, ρ_w is the resistivity of seawater, ϕ is the sediment porosity, a is a constant and m the cementation factor which increases as the grains become less spherical with depth. The latter two parameters can be derived from laboratory measurements of core samples and vary typically between $0.5 < a < 2.5$, and $1.5 < m < 3$. To get an estimate of the hydrate concentration of a deposit, the above formula can be modified to extract the amount of pore space now filled with hydrate from the over-all porosity. The modified formula is

$$\rho_f = a\rho_w\phi^{-m}S_w^{-n}, \tag{2}$$

The parameter S_w is now the pore water saturation factor, n the saturation coefficient and $S_h = (1-S_w)$ is the gas hydrate

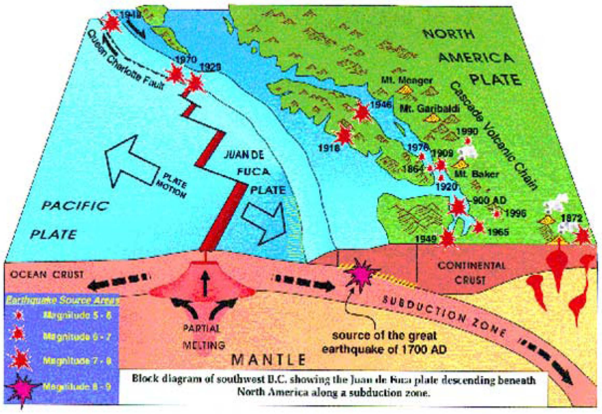

Fig. 4. The tectonics of the Juan de Fuca plate

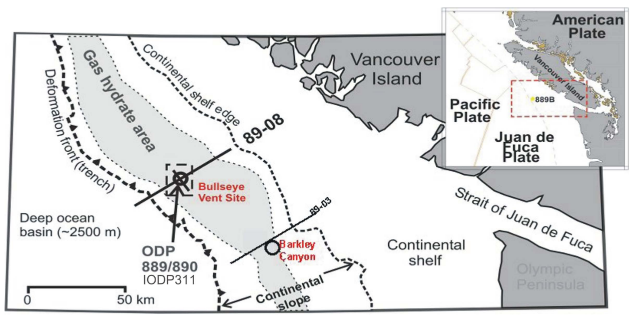

Fig. 5. The location of gas hydrates off on the Cascadia margin, deduced from BSR reflectivity maps.

saturation. A useful description of methods to derive Archie's law coefficients is in e.g.[11]. Typical computed values of shallow marine sediment resistivity range from 1 to 10 Ωm while hydrate may increase these values by a factor of 10 depending on the granular structure.

III. Geological setting - the Juan de Fuca plate and Cascadia

The Juan de Fuca plate extends from the Explorer and Endeavor ridges in the west to the subduction zone beneath the American plate in the east (Fig. 4). Gas hydrates are found on the accretionary prism in close vicinity of ODP Leg 146, Sites 889 and 890, and IODP Expedition 311, Sites U1327 and U1328, as shown in Fig. 5. The Juan de Fuca plate is subducted below the North American plate creating a thick accretionary prism. The presence of gas hydrates on the Cascadia margin were deduced from the BSRs seen on seismic sections acquired in 1985 and the analyses of logs and cores at Site 889, ODP Leg 146 [12] [13]. In the following years, the research effort was intensified in the area and involved single and multi-channel seismic surveys [14] [15] [16], ocean bottom seismometers [17] [18], seafloor compliance [19], electrical resistivity studies [20], [21], and more drilling during IODP Expedition 311 [22]. Several seismic blank zones with diameters between 80 m and 400 m were first observed in deep-towed high-resolution seismic data [23] and later on a 3D multi-channel seismic section [16]. Gas hydrate was found with a piston corer at different locations within the largest of the blank zones. Bullseye Vent, which is the name of the largest blank zone with a diameter of about 400 m on the seafloor, was drilled during IODP Expedition 311 [22]. Useful reviews of gas hydrate studies in this region are given by [24], [25], [26], and the Reports of IODP Expedition 311 [22].

IV. Controlled source EM methods

Controlled source electromagnetic (CSEM) methods depend on a simple concept of physics. If a time varying EM field is generated at or near the seafloor, then eddy currents are induced in the sea water and subjacent crust in accordance with Faraday's law. The outward progress of the currents with time depends on range and electrical conductivity of the surroundings. In particular, the apparent speed in the sea water will be slower than that in the less conductive crustal zones. Measurements at a remote location of the electric and magnetic fields associated with the eddy currents may be inverted for the crustal resistivity structure. The concept is easily verified theoretically through an examination of the governing differential equations. The Maxwell interrelationships between the electric field $\mathbf{E}$ and the magnetic field $\mathbf{B}$ in an isotropic, homogeneous conductive material may be combined as the Helmholtz equation, where the magnetic effects of displacement currents are neglected,

$$-\nabla \times \nabla \times \mathbf{E} = \mu_0 \sigma \frac{\partial \mathbf{E}}{\partial t}, \quad (3)$$

where σ, μ_0 and ϵ are the conductivity, permeability, and permittivity of the material, respectively. A similar equation may be written for the magnetic field vector $\mathbf{B}$. Equation (3) may be rationalized by measuring length and time in units of characteristic length L and characteristic time T where

$$T = \mu_0 \sigma L^2 \quad (4).$$

It the scaled length and time are denoted by prime coordinates, we have

$$-\nabla' \times \nabla' \times \mathbf{E} = \frac{\partial \mathbf{E}}{\partial t'}. \quad (5)$$

A feel for the time taken for an EM disturbance to diffuse through a uniform medium may be gained by evaluating the characteristic time T for a few typical cases. If the scale L is set to 1 km and the parameter μ_0 takes its free space value, then T has value 3.8 s for seawater, typical conductivity 3 S/m, and 1.2, 0.42, 0.12, 0.042 s for crustal resistivities of 1, 3, 10, and 30 Ωm, respectively. The characteristic times T are approximations to the true travel times τ computed accurately for a given model or measured in a survey. T and τ may differ by a factor of 10 or more A straightforward, simple illustration of how time-domain EM systems would respond to a resistive gas hydrate deposit, is presented in Fig. 6. Electromagnetic fields are generated by a seafloor transmitter (Tx) and detected later at a receiver (Rx). The hydrate deposit illustrated in this schematic diagram has the geomety on a cold vent like those seen in Cascadia. Within the roughly cylindrical region, we

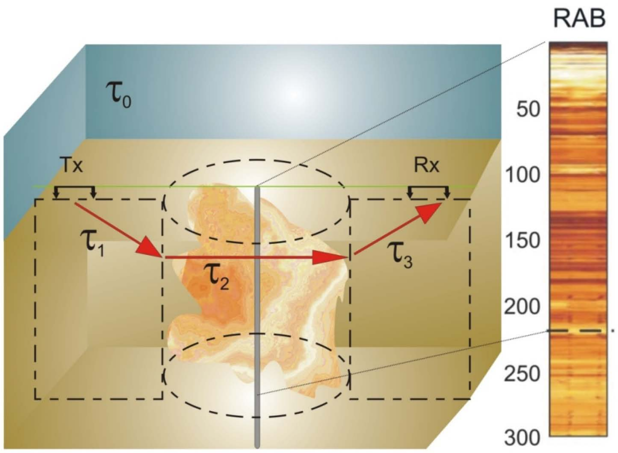

Fig. 6. The superposition of delay times

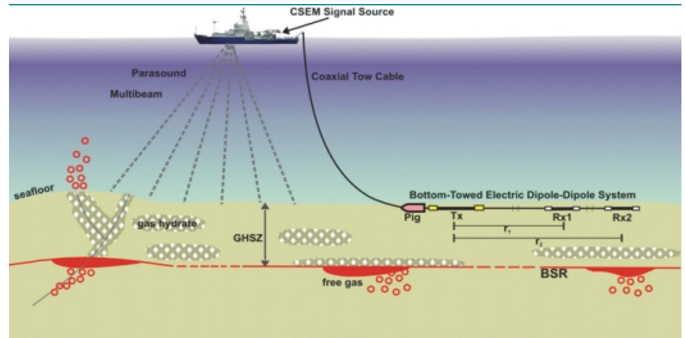

Fig. 7. The towed electric dipole-dipole seafloor CSEM configuration

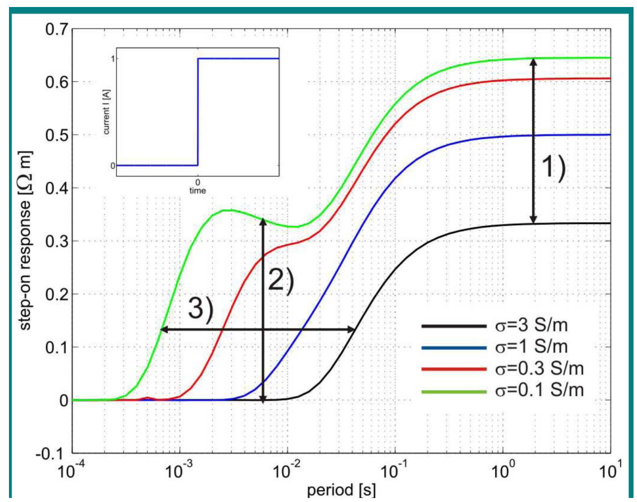

Fig. 8. The step response of a double half-space model to a dipole-dipole system. The separation o the transmitter and the receiver is 100m

suppose some distribution of sediments, pore fluids and gas hydrates which in an average sense, have bulk resistivities different from the environment. The total delay time τ taken for signals to propagate from transmitter to receiver, comes from the sum of delay times for three regions: fore of the vent, inside the vent and aft of the vent [27]. We have

$$\tau = \tau_1 + \tau_2 + \tau_3. \tag{6}$$

The much slower delay time through the seawater is designated τ_0 on Fig. 6 . It is interesting to note that the characteristic time is weighted as the conductivity, or the inverse of resistivity (consider Equation 4). Consequently, whenever measurements are made straddling a resistive anomaly and the background region, the conductive region outside the anomaly will bias any estimated resistivity [28]. The summation in Equation (4) is not influenced by 3D structure outside the zone between the Tx and Rx [27].

V. The Electric Dipole-Dipole System and Specific Theory

A proven CSEM survey method is to tow an inline electric dipole-dipole system to reveal the resistivity structure of the seafloor, as shown in Fig. 7. A time varying current is generated between two transmitter electrodes and voltages are received later at one or more receiver dipoles. The simplest useful theoretical model for which there is a closed form solution is the response of a dipole-dipole system is that of a double-half space, as illustrated in Fig. 8. The theory is developed in a number of papers including Chave and Cox [29], Cheesman, Edwards and Chave [31], Edwards and Chave [30] and Edwards [32]. The upper halfspace is assigned a uniform seawater conductivity of 3 S/m, while the lower half space has crustal conductivities of 3, 1, 0.1 and 0.3 S/m, respectively. Fig. 8 shows the inline step-on responses derived for these different models. The vertical axis has been scaled to yield the DC apparent resistivity at late time. The horizontal axis is in logarithmic time for a transmitter-receiver separation L of 260 m. The curves have three characteristics from which the conductivity of the crust may be obtained. There is late-time variation in amplitude, (Label 1), which is less sensitive with increasing conductivity contrast. There is an early time change in amplitude which depends on the sea floor conductivity, (Label 2). The location in time of this initial change is a strong function of seafloor conductivity (Label 3). It is well known that the late time amplitude variation can be converted to an apparent resistivity which forms the basis of the DC resistivity method. An alternative, more robust estimate, which seems to work well over 2D and 3D structures, can be obtained from the shape and location of the response at early time. One can identify the time at which the step response curve passes through 25% of its maximum value, or equivalently, the maximum in the linear time derivative of the step response. The apparent resisitivity formula can be inferred from the definition of characteristic time T in equation (4). It is

$$\rho_a = C\mu_0 L^2/\tau, \tag{7},$$

where τ is a true travel or delay time. In accordance with geophysical convention, the apparent resistivity formula, the right hand side of equation (7), depends only on field mea-

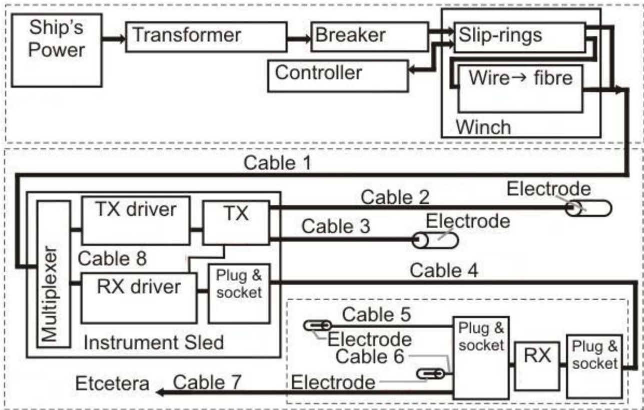

Fig. 9. A block diagram of a towed elctric dipole-dipole system

Fig. 10. The transmitter electronics. The package fits in a pressure vessel about 1 metre long

surements and not on any assumed resistivity model. The exception is the value of C, which is usually selected so that correct results are obtained for a uniform half-space. To get our value of C we have to assume a double half-space model and obtain estimates of it from the equations given in [30]. From the derivative of the step-on response with respect to linear time (which gives the impulse response), making the approximation that water conductivity is much much greater than seafloor conductivity, an analytical value for C can be found as $C = 9 + \sqrt{41} = 15.4$. This value is the upper bound of C. For the range of conductivities of seafloor that we encounter numerically evaluated values lie in the range $13.5 < C < 14.5$.

VI. Apparatus

The apparatus used by our group to successfully map hydrates is described by Yuan and Edwards [20], and Schwalenberg and others [21]. A new system is currently being developed at the University of Toronto to overcome some of the limitations of Yuan and others [33]. There is a patent pending (Edwards and others, [34]). A block diagram of the system is shown in Fig. 9. A similar towed system is currently being developed at the Federal Institute for Geosciences and Natural Resources (BGR), Hannover, Germany. The apparatus consists of a multi-kilowatt power supply. Current flows through the slip rings of the winch into the main tow cable C1. Also connected to the front end of the tow cable at the winch is the communication/data recovery computer. Communications are by copper wire twisted pair converted after the slip rings to fibre optics for transmission to the seafloor. The cable C1 can be several kilometers long. At the lower end it is attached to a heavy sled and plugged into the Tx electronics, Fig. 10. There are power connections to the main unit and communications fibres to the Tx driver. The operation of the Tx is controlled from the ship using an Ethernet protocol. Also in the sled is a Rx driver that derives power from the Tx, talks independently to the ship and monitors voltage signals from the receivers and the corresponding transmitter current simultaneously in real time. The receiver array is modular. It may be assembled in sections each of a different length to build up, for example, a logarithmically-spaced array. Each section has a main cable C4 containing power and communication lines. The Rx electronics are in a small light pressure vessel. The remaining parts of the system consist of Tx and Rx electrodes on cables C2-C3 (typically 5m and 100m), and C5-C6, (2m and 12m), respectively. In practice, the whole system is assembled by plugging together individual receiver sections to form a streamer up to several kilometers long. The streamer is deployed over the stern of the ship, then the sled and finally the tow cable. The array is grounded to the seafloor by the heavy sled and towed in direct contact with the seafloor. Data are collected and may be interpreted to a simple model of the seafloor in real time. While data may be collected preferentially by stopping the array periodically by a process of paying out tow cable from the winch at an observation site and then recovering the cable before the ship arrived at the next site, they can be collected continuously. The advance that enables continuous collection is the 24 bit dynamic range of the Rx amplifier. The high dynamic range means that small signals can be recorded linearly in the presence of streaming potential noise. The signal may then be recovered from noise by a simple stacking process. The Rx amplifier contains no analog filters so the DC limit is recorded correctly, improving interpretation using conventional resistivity methods. The transmitted current and received voltages are digitized simultaneously in the Rx controller so that timing errors are minimal. The transmitter is a type of class D analog amplifier. It is capable of transmitting virtually any waveform sinusoids, square waves, PRBS, etc. Both the Tx and Rx array are fully controllable from the surface. The system may be deployed for many days at a time. The Tx electrodes are designed with water tight connectors which prevent exposure of the ends of cables C2 and C3 to seawater obviating corrosion. The design of the Rx electrodes minimizes streaming potentials.

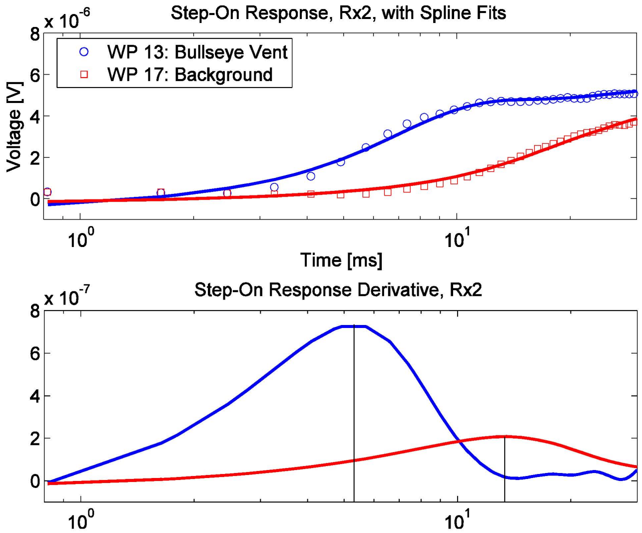

Fig. 11. The upper panel shows the step-on response over the Bullseye Vent, way-point 13 (blue circles with spline fit) and away from the vent, way-point 17 (red squares, with spline fit). The lower panel shows the time derivative of the spline fits, with selected delay times.

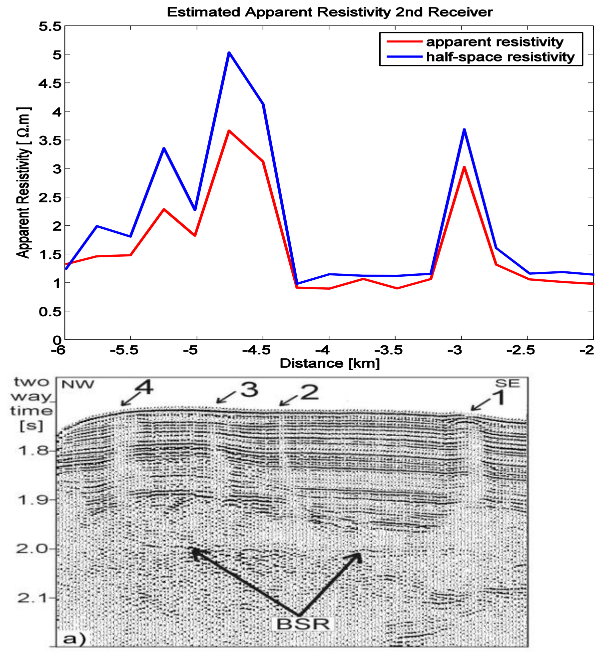

Fig. 12. The upper panel shows the apparent resistivities calculated from the delay times according to Equation (7) along the Profile (1) as well as resitivities determined by fitting a double halfspace model (after Schwalenberg and others [21]. The lower panel shows the reflection seismic data with the four blank zones (BZ1 BZ4).

VII. Cascadia data and their interpretation

Returning to Cascadia, two representative examples of the measured step-on response curves are shown in the upper panel of Fig. 11, for the background region away from the vents and over the Bullseye Vent, respectively.

Compare this figure with Fig. 8. A strong resistivity anomaly is evident. The lower panel shows the linear time derivative of these two response curves. The measured delay time is defined as the position of the peak in the time derivative of the response curve. We then apply Equation (7) to determine the apparent resistivity, shown in Fig. 12

The anomalous peaks in apparent resistivity coincide with the four prominent blank zones [16] observed in the vent field over an area of roughly 1 km by 3 km, as shown in Fig.13. Schwalenberg and others [21] went further, and fit the data to a double half-space model, an entirely reasonable approach as it is the simplest possible model that might explain the data. Certainly, when the array is entirely over the anomalous zone, the half-space model should give the resistivity of the zone provided there are no major features outside the zone between the Tx and Rx. Likewise when the array is entirely over normal sediment, the half-space model should give the background resistivity. We hasten to point out, that the resistivity measured is not indicative of a constant homogeneous resistivity, but is the bulk resistivity of a heterogeneous material. When the array is in an intermediate position, for example over a lateral contact between two dissimilar materials, it is impossible theoretically to fit the broadband data with any 1D structure. It is possible to fit the late time data or the early time data, separately, to a 1D model, but not both simultaneously. So, why is there a strong agreement between the apparent resistivity calculated from just the time delay and the resistivity obtained from the

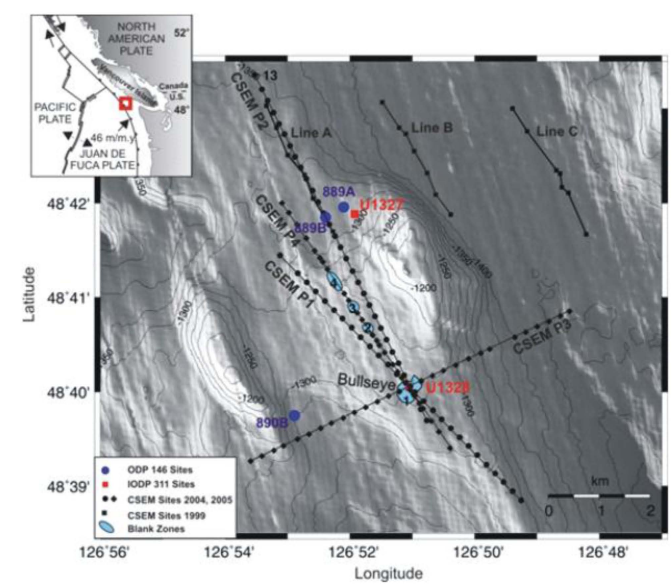

Fig. 13. Map of CSEM Cascadia gas hydrate surveys. The inset map shows the regional tectonics. The bathymetric map shows the position of tow-lines and way points with respect to seismic blank zones including the Bullseye vent (shown in pale blue) and nearby scientific drilling by ODP and IODP. The results of surveys along lines A, B, and C were reported by Yuan and Edwards [20] and the results of surveys along lines CSEM P1 -4 were reported by Schwalenberg and others [21].

half-space inversion? Schwalenberg and others had to apply a lowcut filter to the data for experimental reasons, so they removed the late time data and their half-space models were essentially determined only by the early time data, making the inversion entirely consistent with the apparent resistivity calculation [21]. Can we predict the effects of lateral variations on the resistivity curves? As demonstrated previously, when the CSEM array straddles a vertical contact, the apparent resistivity is biased by the conductive side. Consequently, the breadth of the apparent resistivity anomaly underestimates the width of any resistive target. Thus, our anomaly gives a minimum diameter for the gas hydrate rich cold vent volume.

VIII. Assessment of gas hydrate

Yuan and Edwards [20] were the first to attempt to assess the amount of gas hydrate present in Cascadia using the CSEM method. Their approach was to tow the CSEM array in three distinct regions. One had a strong BSR, the second no BSR, the third was the transition between these zones. Apparent resistivities derived from the data collected on the three lines (A,B, and C on Fig. 13 showed that the resistivity of the seafloor is remarkably uniform over the whole survey area. Yet many of the resistivity values were higher than one would expect for a gas hydrate-free region. In order to interpret their results they had to introduce a gas hydrate distribution, based on early ODP electrical logs from Sites 888 and 889, for a region extending from the seafloor to the base of gas hydrate stability. Using a differential method they then estimated the gas hydrate content with respect to a gas hydrate-free background region of the whole volume from their limited dataset. The average gas hydrate concentration deduced was about 17-26% of pore space (9-13% of sediment volume) in the 100 m interval above the BSR. The values are consistent with, but slightly higher as those obtained by other analyses (e.g. [25]). Further, the presence of gas hydrate was predicted in a region to the east of Site 889B where there is no visible BSR. The total solid hydrate volume estimated within the 10 km survey area was 1.3×10^8 cubic metres. Estimates from more recent surveys are possibly more reliable because of the more pronounced variations in apparent resistivity along the survey lines. The resolution of the CSEM method does not permit a detailed analysis of the distribution of the resistive elements within the blank zones but it does provide an integrated value. Depth resolution is CSEM surveys is difficult because of the lateral moving nature of the fields. Assuming that the increase in resistivity is due to a higher gas hydrate concentration, the latter may be converted to total mass of gas hydrate and then to total available methane. A rough estimate can be made for the Bullseye Vent assuming a cylindrical volume, with diameter and depth of 400 m and 200 m respectively. By using a second differential method, Schwalenberg and others [21] were able to estimate the porosity filled by gas hydrate in the anomalous zones. A baseline concentration derived from the background resistivities was subtracted from the respective profiles, and they found the additional amount of gas hydrate required to

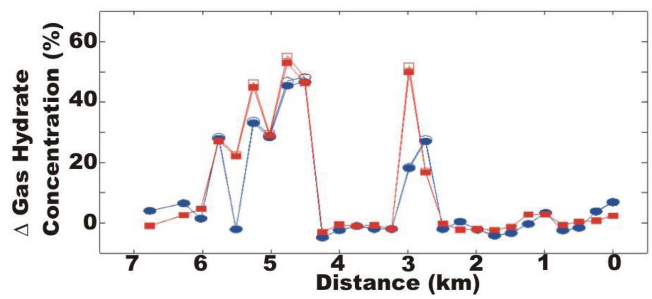

Fig. 14. Gas hydrate concentrations derived from Archie's law using two different sets of Archie coefficients. The first set (a=1.4, m=1.76, n=m) is based on core data from ODP Leg 146 [37]. A re-evaluation of these log data yielded a different set of parameters (a=1, m=2.8, n=1.94) [38]. Blue and red lines and symbols correspond to TX-RX1 and TX-RX2 separations, respectively. In this figure a regional gas hydrate concentration profile derived from the baseline resistivities in Figure 12 has been subtracted from the total gas hydrate concentrations. Thus, the profiles represent the additional amount of gas hydrate and are coincident for both sets of Archie coefficients (after Schwalenberg and others, [21]).

explain the anomalous resistivities appeared to be relatively insensitive to the set of coefficients used, as shown in Fig. 14

They found the additional concentration was more than 50% at maximum and about 25% on average of the available pore space at the Bullseye Vent. Twenty five percent of the available pore space corresponds to 3.8 million cubic meters. With a solid to gas ratio of hydrate of 1:164, the related methane gas volume at STP is 0.62 billion (US) cubic meters. Because of the argument presented above, about the breadth of resistive anomalies sensed by CSEM methods, this may in fact be underestimating the size of the gas hydrate-rich zone.

IX. The Neptune Canada experiment

The Neptune Canada experiment is designed to monitor the Bullseye hydrate deposit over a period of time, possibly many years. The objective is the understanding of how hydrate is formed and how the deposit evolves. Neptune Canada is the first large scale deep ocean observatory system. It has an all-inclusive webpage covering the infrastructure namely power transmission, communication and data management, and the science experiments spanning oceanography, marine chemistry, biology and geophysics [35]. All the data collected are open file and can be downloaded by individuals at their desktop computers. Further, some of the experiments, like the CSEM experiment, can be controlled remotely.

The Neptune observatory network is shown in Fig. 15. It consists of a ring cable linking several nodes to a terminal on Vancouver Island. The nodes labelled Middle Valley and Endeavour are sites where mid-odean ridge processes are studied. The gas hydrate sites are Barkley Canyon and our site at ODP 889. The main cable carries power, a DC sea water return system, and a multi-fibre communication bundle. The power source at the shore station supplies 10kV at up to 10 A. Modified telecom branching units are used to connect nodes to the main cable. The node electronics and its trawl resistant sea floor packaging are shown in Figs. 16 and 17.

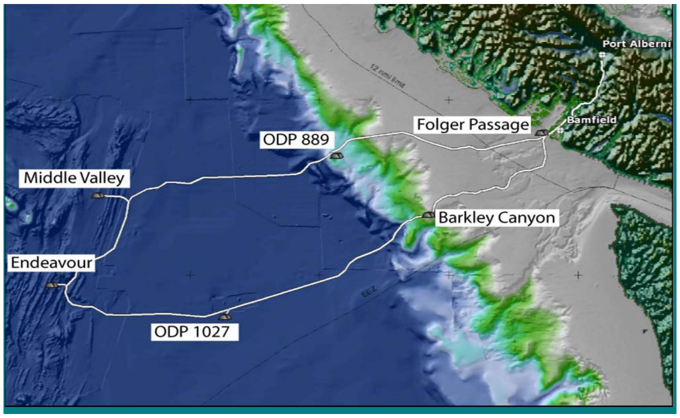

Fig. 15. The Neptune Canada network: a series of nodes connected by a main cable to a shore base station

Fig. 16. The node electronics under testing at Alcatel (Neptune Canada Photograph)

Fig. 17. The trawl resistant packaging for the node (Neptune Canada Photograph)

The nodes supply 400V at 25 A to several junction boxes where the high voltage is converted to 400, 48, 24 and 15 V to feed individual instruments. The communication network is essentially a modified ethernet sytem.Instruments can have their own IP address, like the CSEM, or be connected to serial ports.

A map of the CSEM experiment installed near Bullseye is shown in Fig. 18. The transmitter electronics are very similar

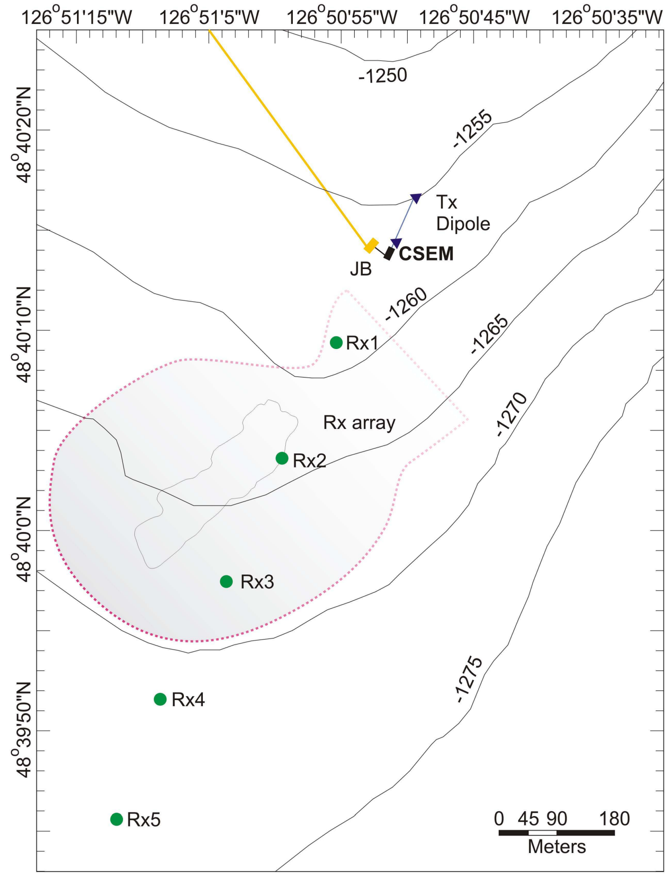

Fig. 18. The CSEM array deployed near the Bullseye vent. The transmitter and receivers are lablelled TX and RX.The transmitter dipole is 100 m long: the receiver array 1000 m long. The junction box for power and communication is labelled JB

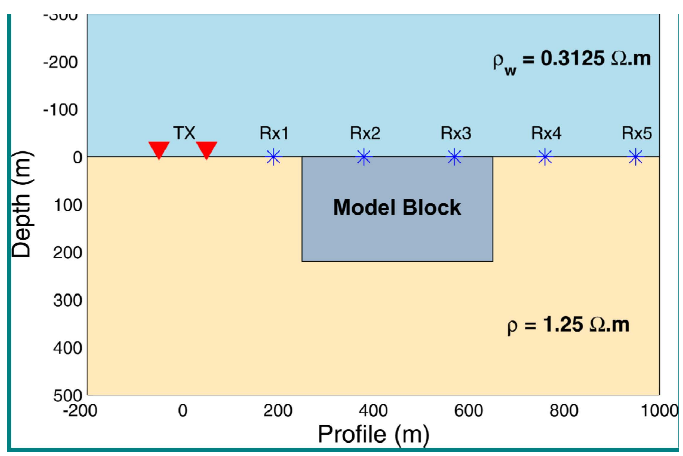

Fig. 19. The theoretical 3D model used to simulate the EM response of Bullseye

to the device described earlier in this paper except the input voltage is 400 VDC rather than three phase AC. The array crosses the surface projection of the seismic blank zone. The topographic expression of Bullseye is significantly smaller than this area (Charles Paull, personal communication). Our

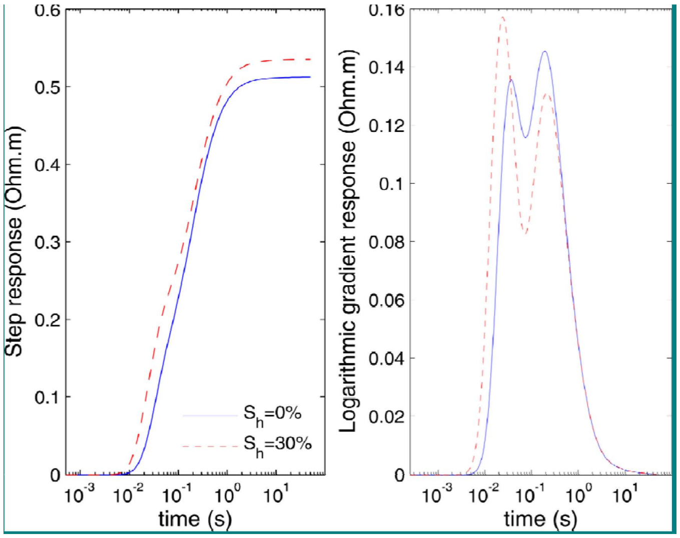

Fig. 20. The step and derivative responses at station RX3 for hydrate concentration in the anomalous zone of 0 and 30%.

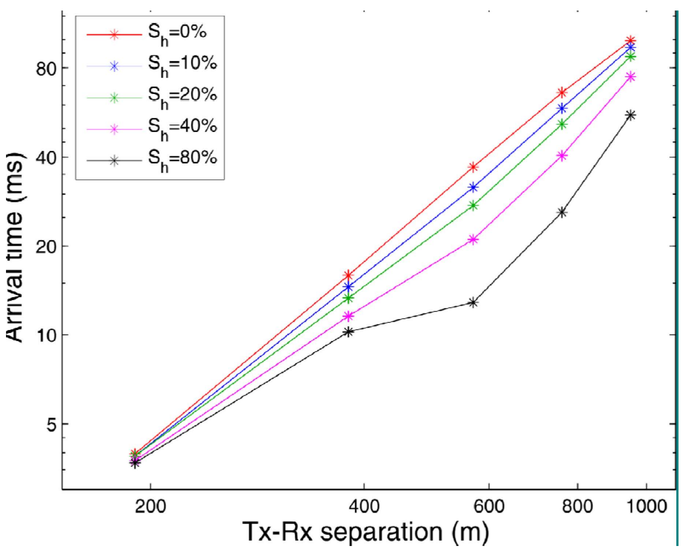

Fig. 21. Variation in delay times across the model for a range of hydrate concentrations

best guess of the geological strike of the extended zone is roughly at right angles to the CSEM array, a line joining the four vent sites..

EM responses of a three dimesional numerical model of the target, Fig. 19, were computed to estimate the effect of varying hydrate content. The software used was written by Druskin and Knizhnerman [36]. The pair of triangles denotes the 100m transmitter dipole and the stars represent receivers. The distance between adjacent receivers is 190 m. The array is on the seafloor at a water depth of 1300m with the seawater having a resistivity of 0.3125 Ω m. The normal, background seafloor has resistivity 1.25 Ω m which corresponds to soft sediment with no hydrate content ($S_h = 0$) with other Archie parameters assigned values: $m = n = 2, a = 1$, and $\phi = 0.5$. The 3D model block, which contains methane hydrate is 400m long (into the paper), 400 m wide and 220m deep. The vertical extent of the structure corresponds to the typical depth of BSR in the area. The resistivity of this structure is changed according to Archies law, given varying amounts of hydrate concentration in pore space.

The DC-normalized transient step-on response and the logarithmic gradient response for RX3 for 2 different models is shown in Fig. 20. The cases for the model block containing no hydrate and a hydrate concentration of 30% of the pore space are compared. The difference in delay time between the two models is a measurable 10 ms. Whether more subtle temporal changes of a few per cent can be resolved is an open question and will depend on the quantity and quality of the data.

Profiles of arrival-time as a function of receiver location for model blocks with different hydrate content are shown in Fig. 21. The upper curve for the non-hydrated model is a line with a slope of 2, indicating that the arrival time is proportional to the square of TX-RX separation for a constant conductivity crust. All other curves show reduced delay times for receivers 2-5 as the model block increases in hydrate content and becomes more resistive. The individual curves change slope at larger offsets where the receiver array becomes sensitive to the resistive material. The largest changes in delay time occur for RX4 and RX5 because a relatively larger percentage of the resistive volume is sampled by these receivers. In contrast, RX1 is almost insensitive to any changes in the model as can be expected, since the current system from the transmitter interacts with the resistive model block after arriving at this receiver.

X. Conclusion

In the last decade, marine controlled source electromagnetic (CSEM) surveys have shown their utility for the characterization of marine gas hydrate targets. We have described the underlying fundamentals of the physics using dimensional analysis. An apparent resistivity formula was introduced, suitable for the display of field data over 1D, 2D and 3D structures. The northern Cascadia area, offshore British Columbia, was selected to demonstrate both the towed CSEM system and the information that can be gleaned from a towed survey including commercial estimates of gas hydrate content. We have not dwelt at length on numerical methods - suffice it to mention there are 1D, 2D and 3D programs available for analysis of multi-receiver CSEM data. CSEM should be used in conjunction with other methods. While a CSEM survey usually gives complimentary results it can yield the unexpected, like the presence of gas hydrate in the absence of a BSR. We have introduced the Neptune Canada experiment, the monitoring of the Bullseye vent over an extended period. Model computations of the response of Bullseye fo the array have been described but the expected changes in the hydrate content with time are really unknown at this stage. We await the switch–on of the Neptune experiment later this year.

Acknowledgments

We thank Peter Hurley and Shuqing Li for their assistance with the design and engineering of the CSEM systems. We thank Kelly Callaway of Fugro, the crew of *J.P Tully* and the pilots of *ROPOS* for their assistance with the marine program. We acknowledge the financial and in-kind support of the Natural Sciences and Engineering Council of Canada, the Geological Survey of Canada, Neptune Canada and in particular the Shell Game Changer program through our scientific advisor Dr. Johannes Singer.

References

[1] E.D. Sloan Jr. *Clathrate hydrates of natural gases*, New York: Marcel Dekker Inc., 1990.

[2] K.A. Kvenvolden, G.D. Ginsburg and V.A. Soloviev. "Worldwide distribution of subaquatic gas hydrates." *Geo-Marine Letters*, vol. 13, pp. 32-40. 1993.

[3] K.A. Kvenvolden. "Methane hydratea major reservoir of carbon in the shallow geosphere?." *Chemical Geology*, vol. 71, pp. 41-51, 1988.

[4] K.A. Kvenvolden and L.A. Barnard. "Gas hydrates of the Blake Outer Ridge, site 533, DSDP Leg 76" *Initial Reports Deep Sea Drilling Project, US Government Printing Office*, vol. 76, pp. 353-365, 1983.

[5] T.H. Shipley, M.H. Houston, R.T. Buffer, F.J. Shaub, K.J. McMillen, J.W. Ladd and J.L. Worzel. "Seismic evidence for widespread possible gas hydrate horizons on continental slopes and rises." *Am. Assoc. Petr. Geol. Bull.*, vol. 63, pp. 2204-2213, 1979.

[6] R.S. White. "Seismic bright spots in the Gulf of Oman."*Earth and Planet. Sci. Lett.*, vol. 37, pp. 29-37, 1977.

[7] R.E. Sheriff. "Factors affecting seismic amplitude."*Geophys. Prosp.*, vol. 23, pp. 125-138, 1975.

[8] M.W., Lee, D. R. Hutchinson, W. P. Dillon, J. J. Miller, W. F Agena, and B. A. Swift. "A method of estimating the amount of in situ gas hydrates in deep sea marine sediments," *Marine and Petr. Geol.*, vol. 10, pp. 493499, 1993.

[9] T.S. Collett. "Detection and evaluation of natural gas hydrates from well logs", Prudhoe Bay, Alaska: MS thesis, Univ. of Alaska, Fairbanks, 1983.

[10] G.E. Archie. "The electrical resistivity log as an aid in determining some reservoir characteristics." *Journal of Petroleum Technology*, vol. 5, pp. 1–8, 1942.

[11] T. S. Collett, and J. Ladd. "Detection of gas hydrate with downhole logs and assessment of gas hydrate concentrations (saturations) and gas volumes on the Blake Ridge with electrical resistivity log data", in C. K. Paull, R. Matsumoto, P. J. Wallace, and W. P. Dillon, eds., *Proceedings of the Ocean Drilling Program, Scientific Results*, vol. 164, pp. 179 191, 2000.

[12] R. D. Hyndman, and E. E. Davis. "A Mechanism for the Formation of Methane Hydrate and Seafloor Bottom-Simulating Reflectors by Vertical Fluid Expulsion", *J. Geophys. Res.*, vol. 97(B5), pp. 70257041, 1992.

[13] Westbrook, G. K., B. Carson, and R. J. Musgrave, "Proceedings of the Ocean Drilling Program, Initial Report, Part 1", vol. 146, Ocean Drilling Program: College Station, Texas, 1994.

[14] T. Yuan, R. D. Hyndman, G. S. Spence, and B. Desmons. "Seismic velocity increase and deep-sea gas hydrate concentration above a bottom-simulating reflector on the northern Cascadia continental slope." *Journal of Geophysical Research*, vol. 101, pp. 13655-13671, 1999.

[15] C. R. Fink, and G. D. Spence. "Methane hydrate distribution offshore Vancouver Island from detailed single seismic reflection data." *Journal of Geophysical Research*, vol. 104, pp. 2909-2922, 1999.

[16] M. Riedel, G. D. Spence, N. R. Chapman, R. D. Hyndman. "Seismic investigations of a vent field associated with gas hydrates, offshore Vancouver Island." *Journal of Geophysical Research*, vol. 107, (B9), doi:10/1029/2001JB000269, 2002.

[17] J. W. Hobro, S. Singh, and T. A. Minshull. "Tomographic seismic studies of the methane hydrate stability zone in the Cascadia margin." *Geological Society of London Special Publication*, vol. 137, pp. 133-140, 1998.

[18] G. D. Spence, T. A. Minshull, and C. R. Fink. "Seismic studies of methane hydrate, offshore Vancouver Island." *Proceeding of the Ocean Drilling Program, Scientific Results*, vol. 146, pp. 163-174, 1995.

[19] E. C. Willoughby and R. N. Edwards. "Shear Velocities in Cascadia from Seafloor Compliance Measurements." *Geophysical Research Letters*, vol. 27, pp. 1021-1024, 2000.

[20] J. Yuan, and R. N. Edwards. "The assessment of marine hydrates through electrical remote sounding: Hydrate without a BSR." *Geophysical Research Letters*, vol. 27, 16, pp. 2397-2400, 2000.

[21] K. Schwalenberg, E. C. Willoughby, R. Mir, R. N. Edwards. "Marine gas hydrate electromagnetic signatures in Cascadia and their correlation with seismic blank zones." *First Break*, vol. 23, pp. 57-63, 2005.

[22] M. Riedel, T.S. Collett, M.J. Malone, and the Expedition 311 Scientists, Proc. IODP, 311: Washington, DC: (Integrated Ocean Drilling Program Management International, Inc.). doi:10.2204/iodp.proc.311., 2006

[23] W. T. Wood, D. A. Lindwall, J. F. Gettrust, K. K. Sekharan, and B. Golden. "Constraints on gas or gas hydrate related wipeouts in seismic data through the use of physical models: EOS, Trans., American Geophys. Union, 81, (48), F639. Wood, W. T., J. F. Gettrust, N. R. Chapman, G. D. Spence, and R. D. Hyndman, 2002, Decreased stability of methane hydrate in marine sediments owing to phase boundary roughness." *Nature*, vol. 420, pp. 656-660, 2000.

[24] R. D. Hyndman, G. D. Spence, N. R. Chapman, M. Riedel, and R. N. Edwards. "Geophysical Studies of Marine Gas Hydrate in Northern Cascadia", in C. K. Paull and W. P. Dillon, eds.,*Natural gas Hydrates, Occurrence, Distribution and Detection, Geophysical Monograph Series No. 124*: American Geophysical Union (AGU), p. 273-295, 2001.

[25] G. D. Spence, R. D. Hyndman, N. R. Chapman, M. Riedel, R. N. Edwards, and J. Yuan, 2000, "Cascadia Margin, northeast Pacific Ocean: hydrate distribution from geophysical investigations", in M. D. Max, ed., *Natural Gas Hydrate in Ocean and Permafrost Environments*: Kluwer Academic Publisher, p. 183 198.

[26] M. Riedel, I. Novosel, G. D. Spence, R. D. Hyndman, R. N. Chapman, R. C. Solem, and T. Lewis. "Geophysical and geochemical signatures associated with gas hydrate related venting at the north Cascadia Margin." *GSA Bulletin*, vol. 118, no. 1-2, pp. 23-38; DOI: 10.1130/B25720.1, 2006.

[27] M.E. Everett, R.N. Edwards, S.J. Cheesman, H. Utada, and I.J. Ferguson. "Interpretation of seafloor electromagnetic data in applied geophysics." *Applied Electromagnetics in Materials* , Oxford: Permagon, 1988.

[28] R. N. Edwards, K. Schwalenberg, E.C. Willoughby, R. Mir and C. Scholl. "Marine Controlled Source Electromagnetics and the Assessment of Seafloor Gas Hydrate." *SEG Publications* Tulsa (in press).

[29] A.D. Chave and C. S. Cox. "Controlled electromagnetic sources for measuring the electrical conductivity beneath the oceans." *Journal of Geophysical Research*, vol. 87, pp. 5327–5338, 1982.

[30] R.N. Edwards and A.D. Chave. "A transient electric dipole-dipole method for mapping the conductivity of the seafloor." *Geophysics*, vol. 51, pp. 204–217. 1986.

[31] S. J. Cheesman, R.N.Edwards, and A.D. Chave. "On the theory of seafloor conductivity mapping using transient electromagnetic systems." *Geophysics*, vol. 52, pp. 204217, 1987.

[32] R.N. Edwards. "On the resource evaluation of marine gas hydrate deposits using a seafloor transient electric dipole–dipole method." *Geophysics*, vol. 62, pp. 63–74, 1977.

[33] J. Yuan, G. Cairns, and R. N. Edwards. "Electromagnetic Assessment of Offshore Methane Hydrate Deposits on the Cascadia Margin." *Eos Trans. AGU, 79, Fall Meet. Suppl.*, Abstract GP22A-08, 1998.

[34] R.N. Edwards, E.C. Willoughby, C. Scholl and R. Mir. "A Continuously Towed Seafloor Electromagnetic Prospecting Systemen." *U.S. Provisional Patent Application 61/122,489*, filed December 15, 2008.

[35] "Neptune Canada", Internet: www.neptunecanada.ca, [March,2010].

[36] V. L. Druskin and L. A. Knizhnerman, "Spectral approach to solving three dimensional Maxwells diffusion equations in the time and frequency domains.". *Radio Science*, vol. 29, pp. 937–953, 1994.

[37] R. D. Hyndman, T. Yuan, and K. Moran. "The concentration of deep sea gas hydrates from downhole electrical resistivity logs and laboratory data." *Earth and Planetary Science Letters*, vol. 172, pp. 167-177, 1999.

[38] M. Riedel, T. S. Collett, and R. D. Hyndman. "Gas hydrate concentration estimates from chlorinity, electrical resistivity, and seismic velocity." *Geological Survey of Canada, Open File Report 4934*, 2005.